Linking hydrological variations at local scales to regional climatic teleconnection patterns

Kabir Rasouli[1], Karis Scharold[2], Taufique Mahmood[2], Nancy Glenn[3], and Danny Marks[4]

[1]Environment and Climate Change Canada Québec
[2]University of North Dakota
[3]Boise State University
[4]USDA-ARS

June 25, 2020

Abstract

Interactions between the land surface and the atmosphere play essential roles in hydrological variations at local scales. Variations of regional climate patterns over preceding years have key effects on the seasonal water and moisture conditions in the following year. The linkage between regional climate and local hydrology is challenging due to scale differences, both spatially and temporally. In this study, multiple hydroclimatic phases were identified to relate climatic teleconnection patterns to hydrological processes in a small headwater basin within Reynolds Creek Experiment Watershed, Idaho, USA. A singular spectrum analysis and a combination of hydrological observations and outputs from a physically based hydrological model were used for this purpose. Results showed that a positive phase of North Atlantic Oscillation (NAO) is more influential than a positive phase of the Pacific North American (PNA) pattern on the observed annual runoff and the modeled rain on snow runoff in the study area. Specifically, we found a 43% and 26% shift below normal in annual runoff and rain on snow runoff from NAO and a 29% and 9% below normal from PNA. More frequent rain on snow events were observed under a positive phase of Antarctic Oscillation, leading to a 45% increase in the rain on snow runoff, which accounts for one-third of the mean annual runoff. A high runoff-to-precipitation ratio was observed in the study area under negative phases of Arctic Oscillation and Sea Surface Temperature in the Niño 3.4 region of the Equatorial Pacific Ocean. A switch in the phase of the teleconnection patterns of NAO and PNA in 2012 was concomitant with a transition from wet to dry conditions in the basin, suggesting the importance of the regional teleconnections in affecting snow and runoff regimes at local scales. The identified hydroclimatic phases can be implemented in operational models to improve uncertainties in hydrological forecasts, climate projections, and water resources planning.

INTRODUCTION

Uncertainty in the representation of hydrological processes at local scales in Earth system models can affect the accuracy of the weather forecasts and climate projections. Water budget and surface energy in large basins, which are formed by small homogenous hydrological response units, are primarily affected by regional climatic teleconnection patterns. Small variations in climatic patterns can lead to large hydrological responses (Whitfield, 2001), and can affect hydrological predictability (Rasouli, Hsieh, & Cannon, 2012). Interactions between local and regional scale hydroclimatic fluxes, however, are not sufficiently resolved in the Earth system and climate models used for environmental change studies (Fan et al., 2019). Whitfield, Moore, Fleming, and Zawadzki (2010) studied the low frequency (e.g., multi-decadal) and high frequency (e.g., monthly) variations of climate and their associations with hydrological changes. A multi-decadal component of spring streamflow, for instance, is associated with variations in spring precipitation and air temperature driven by low frequency atmospheric circulations and sea level pressure (Boé & Habet, 2014). In snow-dominated mountains with shallow soils and high spatial heterogeneity, streamflow variations also depend on low frequency variations of groundwater. Because of the lower velocity of groundwater relative to surface runoff, it can take three to eight years to recycle and contribute to surface flows in mountainous areas, depending on the variability of meltwater from fresh snowpack (e.g., Plummer et al., 2001; Manning et al., 2012). The decomposition of local hydrological time series into its components can yield comparable scales that are needed to relate climate circulations with a low frequency and long cycles to hydrological fluxes with a high frequency and short durations. Understanding hydrological variations with an intermediate frequency (e.g., occurring every 3 – 8 years) remains challenging in mountainous regions with large geological heterogeneity as attribution of antecedent energy and moisture conditions in the previous years to seasonal snow and flow regimes in the following year cannot be easily monitored or estimated. Spatial and temporal variations of snowmelt, runoff, groundwater storage and flow, antecedent soil moisture, snow redistribution by blowing wind, and snow sublimation, are high, which makes modeling and predicting mountain hydrology uncertain (Lehning, Grünewald, & Schirmer, 2011). This becomes even more challenging when hydrological models are forced with atmospheric fluxes with uncertain measurements and large natural variations.

Reynolds Creek Experimental Watershed (RCEW), with a semiarid cool montane climate in Idaho, USA, is of specific scientific interest. For example, its critical zone responses to climate change have been monitored over three decades and subsequently modeled by many studies (e.g. Seyfried, Grant, Marks, Winstral, & McNamara, 2009; Reba et al., 2011a; Kumar, Wang, & Link, 2012; Marks, Winstral, Reba, Pomeroy, & Kumar, 2013; Rasouli, Pomeroy, & Marks, 2015). Reynolds Mountain East (hereafter, Reynolds Mountain), as a headwater basin within RCEW, has been widely investigated to understand hydrological changes in the mountains and often cited in the literature as a representative basin for semiarid snow dominated regions (e.g. Marks & Winstral, 2001; Reba et al., 2011a; Kumar, Marks, Dozier, Reba, & Winstral, 2013; Wang, Kumar, & Marks, 2013; Chen, Kumar, Wang, Winstral, & Marks, 2016). Reba, Marks, Winstral, Link, and Kumar (2011b) conducted a detailed study of the sensitivity of the snow cover energetics and classified hydrological simulations into eight categories based on annual and winter precipitation and snowpack. All eight categories in Reynolds Mountain, however, were temporally discontinuous. Dry and cool conditions, for instance, in 1985 and 2000, may not belong to the same teleconnection phase and may have different atmospheric driving mechanisms. Interactions between local hydrological dynamics and regional climatic teleconnection patterns, along with a physically based representation of these interactions in climate models, can improve the understanding of climate and hydrological processes at local scales (Prein et al., 2015) and the understanding of weather and climate extremes at regional scales (Langendijk et al., 2019). The large biases that weather and climate model outputs show against observations (Fowler, Blenkinsop, & Tebaldi, 2007) can be reduced by linking land surface processes and local atmospheric convection to climatic teleconnection patterns across a range of temporal and spatial scales.

The attribution of regional climate patterns over the preceding years to seasonal hydrological fluxes at local scales in the following year has not been sufficiently understood. Therefore, the linkage between local hydrological processes and regional climatic teleconnections patterns was explored in this study. The linkage between local hydrological variations and climatic teleconnection patterns, assessed over multiple hydroclimatic phases in this paper, can be missed when only seasonal precipitation, snowmelt runoff, and evapotranspiration are investigated. Misrepresenting low (e.g., multiple decades), intermediate (e.g., 3 – 8 years), and high (e.g., multiple months) frequency variations can result in uncertainties in climate projections and failure in both short and long-term hydrological predictions (Dutta & Maity, 2018). This study addresses the following research questions: how do local hydrological processes in a small basin relate to regional climatic patterns, and how does the spatial variability of hydrological fluxes in snow dominated mountain basins differ under different phases of atmospheric circulations?

STUDY AREA AND DATA SOURCES

The study area is Reynolds Mountain in the Owyhee Mountains in Idaho, USA. Reynolds Mountain is a zero-order basin that drains to the Snake River (Figure 1). Reynolds Mountain has a small drainage area (0.38 km^2) and it is characterized by large patches of steep north and west facing slopes (Figure 2c). Elevation ranges in Reynolds Mountain vary between 2028 m and 2137 m. The vegetation is dominated by low, big, and Wyoming sagebrush (*Artemisia arbuscula Nutt., Artemisia tridentata Nutt.* subsp. vaseyana [Rydb.] Beetle and subsp. Wyomingensis, respectively), bitterbrush (*Purshia tridentata* [Pursh] DC), and native and non-native grasses, including cheatgrass (*Bromus tectorum*). Aspen (*Populus tremuloides*), subalpine fir (*Abies lasiocarpa*), and Douglas-fir (*Pseudotsuga menziesii*) communities are found in the water-rich areas such as below drifts and riparian zones. Figure 3 shows a distribution of the sagebrush and forest communities. Soils in Reynolds Mountain are derived from igneous granitic and volcanic rocks and lake sediments.

Reynolds Mountain has been monitored since 1983. The instrumentation includes a streamflow gauge at the basin outlet and two sheltered and exposed weather stations (Figure 1). The meteorological data include hourly air temperature, relative humidity, wind speed, precipitation (snow undercatch-corrected), shortwave radiation, and longwave radiation, which are used to force the hydrological model. The hydrological data include hourly snow water equivalent (SWE) measurements at a snow pillow site and hourly streamflow observations at the basin outlet. A snow pillow was used near the sheltered station to estimate SWE. Reba et al. (2011b) suggest that the snow accumulation at this site is enhanced by the impact of topographic and vegetation sheltering on wind redistribution. On the contrary, Winstral and Marks (2014) showed that SWE measurements at the snow pillow site are representative of the basin averages. The snow pillow SWE measurements and a lidar-derived snow depth product were used in this study for assessing the model performance in capturing the spatial variability of snow accumulation (Shrestha & Glenn, 2016). Lidar-derived snow depths were obtained from processing and then subtracting a snow-free lidar digital elevation model (DEM) from a snow covered DEM in Reynolds Mountain on March 19, 2009.

METHODS

3.1 Hydrological modeling

In this study, a combination of hydrological model outputs and observations were used to investigate linkages between hydrological characteristics at local scales and climatic teleconnection patterns over a large domain. A combination of modeling and observational data were used to comprehensively investigate the linkages because even intensively instrumented watersheds such as Reynolds Mountain do not record all of the necessary water and energy balance fluxes. For instance, measured precipitation, modeled rainfall, modeled snowfall, and measured streamflow or annual runoff were used. To gain confidence in the model used, its performance in simulating snow was assessed.

The cold regions hydrological modeling (CRHM) platform (Pomeroy et al., 2007) has been widely used and tested in various agricultural and mountainous regions in Canada and other cold areas such as the Canadian Rockies, Qinghai-Tibetan Plateau, Patagonia, the Pyrenees and the Alps (Dornes, Pomeroy, Pietroniro, Carey, & Quinton, 2008; Ellis & Pomeroy, 2007; Ellis, Pomeroy, Brown, & MacDonald, 2010; Fang et al., 2013; Lòpez-Moreno, Pomeroy, Revuelto, & Vicente-Serrano, 2013; Mahmood, Pomeroy, Wheater, & Baulch, 2017; Pomeroy, Fang, & Rasouli, 2015; Rasouli, Pomeroy, Janowicz, Carey, & Williams, 2014; Rasouli et al., 2015; Rasouli, Pomeroy, & Whitfield, 2019a, 2019b; Rasouli, 2017). A strength of CRHM is its ability to capture snow redistribution and sublimation, and thus, it provides an understanding of the spatial and temporal heterogeneity of the hydrological processes in snow dominated watersheds. In this study, components of the hydrological water balance were simulated using the CRHM platform. The model was forced with observation data and run on homogeneous hydrological response units (HRUs) to characterize the surface and near-surface cold regions hydrological processes. The model performance in capturing the spatial variability of snow depth was assessed in Reynolds Mountain.

A set of physically based modules describing the major processes were compiled (using CRHM platform) into a watershed model informed by results from previous scientific findings and modeling experiments in research basins (Carey, Quinton, & Goeller, 2007; Dornes et al., 2008; Flerchinger, Reba, & Marks, 2012; Link, Flerchinger, Unsworth, & Marks, 2004; McCartney, Carey, & Pomeroy, 2006; MacDonald, Byrne, Kienzle, & Larson, 2011; Pomeroy, Hedstrom, & Parviainen, 1999; Pomeroy, Toth, Granger, Hedstrom, & Essery, 2003; Pomeroy et al., 2006; Quinton & Carey, 2008; Reba, Pomeroy, Marks, & Link, 2012; Reba, Marks, Link, Pomeroy, & Winstral, 2014; Williams et al., 2015; Winstral, Marks, & Gurney, 2013). The phase of precipitation, whether it falls as snow or rain, was partitioned based on the psychrometric energy balance of the falling hydrometeors and turbulent transfer equations of blowing snow sublimation (Harder & Pomeroy, 2013). Two energy balance snowmelt and evapotranspiration modules were used in the CRHM model. The snowfall and rainfall intercepted on the canopy were estimated and used to calculate the sublimation and evaporation losses. The turbulent transfer to snow and wind-driven snow transport and redistribution were modeled using CRHM to better close the mass balance in the basin. No calibration was applied for snow simulations. Runoff generated during rain on snow (ROS) events was estimated from an energy balance model and calculating advective heat flux from precipitation when snow is on the ground and the equivalent melt from advected heat to snowpack (Marks, Link, Winstral, & Garen, 2001). In the developed model, vegetation height, density, and stalk diameter control the aerodynamic roughness and play a key role in blowing snow transport. Thus, snow is transported from shorter vegetation HRUs such as sagebrush to taller vegetation HRUs such as riparian forest and aspen. The modules and references to the methods used are listed in Table 1. For more details on each module and each hydrological process refer to Rasouli et al. (2014) and Rasouli (2017).

3.2 The spatial arrangement of the hydrological model

The water and energy balance fluxes were modeled for HRUs with hourly time steps. HRUs that act as control volumes of the calculation were spatially segregated based on surface physiographic information relevant for hydrological model parameterization, including vegetation cover, topography, soil depth, soil layers, the variability of basin attributes, and the level of model complexity. A spatially distributed modeling structure was developed with 22 HRUs (Figure 3). HRU configuration was adapted from previous studies (e.g., Newman, Clark, Winstral, Marks, Seyfried, 2014; Rasouli et al., 2015) and extended based on aspect and slope. Drift HRUs in aspen and sage vegetation are in topographic depressions downwind of slope breaks, where deep snow accumulates, which sustain snowmelt water for the trees in spring and early summer.

3.3 Physical parameterization of the hydrological model

Parameter estimation in Reynolds Mountain was based on previous studies in this basin, other headwater basins in RCEW, and similar snow dominated basins. Model parameters adapted from measurements in the research basins to represent the vegetation characteristics, snowmelt, and blowing snow redistribution. A uniform blowing snow fetch distance was used for all HRUs due to the short upwind distance. Blowing snow was inhibited for the sheltered HRUs. Snow surface roughness length was estimated by Reba et al. (2012). Vegetation heights/density and leaf area index were determined by Link et al. (2004), Seyfried et al. (2009), and Flerchinger et al. (2012). The soil characteristics, including soil water storage capacity and the soil surface saturation, were adapted from Seyfried et al. (2009) and Link et al. (2004), respectively. Initial soil temperature was measured by soil thermocouples prior to the major snowmelt. The thermal conductivity value was taken from Oke (1978).

3.4 Classification of hydroclimatic phases

The water balance cycle of a basin cannot be closed unless the effects of hydrological and meteorological conditions in preceding years are taken into account, in addition to the seasonal precipitation and runoff.

There are multiple methods in the literature to break down time series into distinct components that represent different temporal frequencies of the variations (e.g., wavelet transform (Huang et al., 1998) and empirical mode decomposition (Daubechies 1992)). Alexandrov et al. (2012) found the singular spectrum analysis (SSA) method to have the highest performance. We used the SSA method to decompose daily precipitation time series. SSA is typically used for spectral decomposition of a time series, estimating the spectrum of eigenvalues in a singular value decomposition of a covariance matrix. The components of SSA are trend, periodic components, and noise, each having a meaningful interpretation. The basic structure of SSA includes: (1) decomposing the one-dimensional time series into multidimensional series by adding lagged variables and creating a so-called trajectory matrix; and (2) conducting a principal component analysis on the trajectory matrix (Hsieh, 2009).

Precipitation data were used for SSA and to identify the hydroclimatic phases, because it dominates the variability in the water budget of a basin. Precipitation also has seasonality and serial dependencies, which can be decomposed by SSA. The seasonality can be multiple seasons, years, or decades, depending on the nature of the phenomena. The first mode or eigenvector of SSA on precipitation usually shows an intermediate frequency variation, which is ideal for representing hydroclimatic phases with multiple year durations studied herein. The long term average of the first eigenvector of SSA on precipitation is used as the threshold to indicate whether a given hydroclimatic phase shows a wet or dry condition. If the moving average of the first eigenvector of SSA on precipitation is above the long term average for a period of three to eight years, it is defined as a positive hydroclimatic phase, and if it is below the long term average, it is defined as a negative hydroclimatic phase.

Climatic teleconnection patterns represent regional atmospheric and oceanic circulations over multiple years and decades. The teleconnection patterns used in this study are Antarctic Oscillation (AAO), Sea Surface Temperature (SST), Arctic Oscillation (AO), North Atlantic Oscillation (NAO), and Pacific-North American (PNA) pattern. These teleconnection patterns were chosen because large-scale atmospheric circulation changes occur via these teleconnections (Overland & Wang, 2010) and there is evidence of their effects on snow regimes in western North America (e.g., Bao, Kelly, & Wu, 2011). For instance, NAO is one of the most dominant teleconnection patterns in the atmosphere and is similar to AO in describing the difference in pressure gradient between Azores high and Icelandic low in a different time period (Hurrell, Kushnir, Ottersen, & Visbeck, 2003). During the positive phase of NAO, the jet stream blows strongly and consistently from west to east, which locks up the cold and dry Arctic air in the polar region, leading to warm and wet winters in North America. But during the negative phase of NAO, the reduced pressure gradient weakens the westerly wind allowing the cold Arctic air to move to the mid-latitude region (Francis & Vavrus, 2012; Cohen et al., 2014), leading to cold winters in North America. SST in the Niño 3.4 area of the Equatorial Pacific Ocean also can affect ROS events. McCabe, Clark, and Hay (2007) showed that there are more frequent ROS events in the northwestern United States during La Niña conditions than El Niño. Low flow conditions in western North America are also associated with El Niño events and a positive phase of the PNA pattern (Bonsal & Shabbar, 2008). AAO is a large-scale mass transport in the atmosphere between the mid-latitudes and high latitudes (Gong & Wang, 1999).

The climatic teleconnection patterns and anomalies of observed annual precipitation, mean winter air temperatures, the modeled rainfall to precipitation and runoff to precipitation ratios were compared in each hydroclimatic phase against their long term averages. A correlation analysis was also conducted among the meteorological and hydrological variables to determine the importance of the atmospheric teleconnection patterns in small-scale watersheds. We expect that the detected hydroclimatic phases to be aligned with negative or positive phases of the teleconnection patterns, and snow, ROS runoff, and streamflow to behave differently in each phase. As runoff generated during ROS events contributes significantly to the annual runoff, its spatial and temporal variability was examined in detail under different climate phases.

RESULTS

4.1 Snow simulations

The hydrological model performance in simulating SWE is adequate for all winter seasons at the snow pillow site in Reynolds Mountain (Figure 4), which provides confidence that the model can represent snow melt and other fluxes that cannot be easily measured. The Nash-Sutcliffe efficiency (*NSE*), normalized mean bias (*NBIAS*), and root mean squared error (*RMSE*) are 0.95, -0.01, and 4.8 cm, respectively. The cumulative snowfall shown in Figure 4 illustrates the accumulation or loss of snow at the snow pillow site. There is a pronounced difference between cumulative snowfall and peak SWE (Figure 4), indicating the snow depletion by midwinter melting, winter snow redistribution, and sublimation during most of the simulation period. Further diagnosis, using model outputs, suggests that melting processes during midwinter and early spring are responsible for large snow depletion due to a series of warm spells having a maximum air temperature of ~10 oC. For example, during 1983-84 winter, five warm spells (one week duration each) occurred with a mean air temperature of 5 oC that resulted in melting 176 mm of SWE before it peaked on April 15, 1984.

The simulated spatial snow depth agrees well with the observed snow depth from airborne lidar (Figure 5; Table 2). The spatial *NSE*between observations and simulations is 0.7 for all HRUs. The mean of observed and simulated spatial snow depths are 0.99 m and 1.03 m, respectively. The model captures the areas of snow sinks and sources with reasonable error ranges (Figure 5). Both simulated and observed snow depth maps provide the first sign of underlying spatial controls on the distributed snow processes. The snowpack usually recedes markedly in almost 50% of the basin by mid-March. Snowpack in HRUs with north facing aspects and forest cover (Figure 2c, Figure 3), however, does not reach the peak value (Figure 5). Table 2 shows that sagebrush and aspen HRUs having north facing steep slopes have high snow depths as these areas have slow snow depletion rates with low solar radiation and receive transport of snow from other HRUs. For example, a total sunshine period during 2008-2009 winter for north facing steep slopes in sagebrush is 45 days, which is lower than that of the east facing sagebrush regions (66 days). Aspen and riparian forest on flat-lying areas in the valley bottom also experience high snow accumulations as snow is redistributed from sagebrush and grassland areas to wooded areas in both basins.

Modeled net blowing snow transport into the riparian forest is up to 62 mm, which is 10% of the 2008-09 total precipitation. In contrast, the blowing snow transport from the sagebrush HRU is 32 mm. Thus, vegetation type or height, aspect, slope, and topographic depressions play an essential role in the spatial variability of snow accumulation. Previous studies (Reba et al., 2011a; Kumar et al., 2013; Rasouli et al., 2015) emphasized the impacts of vegetation induced blowing snow transport as a major process responsible for the spatial variation of SWE. Vegetation, aspect, and slopes are found as partial factors affecting the spatial variation of snow accumulation at a regional scale in western North America (Tennant et al., 2017).

4.2 Relation between climatic teleconnection patterans and local hydrology

The Pearson correlation coefficients were calculated between basin-scale hydrological variables, including observed mean annual and winter air temperatures, modeled annual rainfall, the ratio of modeled rainfall to observed precipitation, modeled snowfall, observed annual runoff, the ratio of annual runoff to total annual precipitation, observed peak SWE and its timing in Reynolds Mountain, and teleconnection patterns (Figure 6). The partitioning of precipitation into rainfall and snowfall was used to calculate the ratio of rainfall to total precipitation, which showed the strongest relation with AAO in the same year with a correlation coefficient of -0.7 (Figure 6a). The ratio of rainfall to precipitation also has an intermediate positive correlation with SST (Figure 6b) and a strong negative correlation with PNA in the preceding year (Figure 6e). The climate teleconnection of NAO showed an intermediate positive relation with winter air temperature and a negative relation with the annual ROS runoff (Figure 6d).

Six major hydroclimatic phases with distinct climatic conditions were identified based on the decomposed multiple year frequency time series of daily precipitation (Figure 7). Each phase was classified into a wet or dry (above or below average, respectively) span, lasting for three to eight years. Characteristics of the identified hydroclimatic phases (Figure 7) in relating the hydrological variables and climatic teleconnection patterns are demonstrated in Figure 8. Phase (1) is a wet and cold period under negative AO and SST from 1984 to 1986; phase (2) is a dry and warm period from 1987 to 1994 under positive AO and NAO; phase (3) is a wet and cold period from 1995 to 1999 under positive AAO; phase (4) is a warm period from 2000 to 2003 under the SST transitioning from negative to positive and positive PNA; phase (5) is in a transition from warm to cold conditions under positive PNA and negative NAO from 2004 to 2011; and finally, phase (6) is a low flow period from 2012 to 2014 under negative PNA and positive NAO.

4.3 Time variation of rain on snow (ROS) events

The hydrological importance of ROS events in generating high flows and its potential relation with NAO and AAO, warrants studying these events in more detail for different snow regimes in Reynolds Mountain. Snowmelt generates substantial runoff during ROS events. The ROS contribution to total runoff, however, depends on (i) snow cover of the HRUs and (ii) rainfall occurrence. Heterogeneity of snow cover due to topography and redistribution of snow by wind controls the runoff during ROS events. Snow transport to sinks and topographic depressions with drifted snow can intensify snowmelt in spring, and early summer when the likelihood of rainfall is high.

HRUs with drifted snow have deep snowpacks (Figure 5) and generate high ROS runoff depths and contribute more than other HRUs to basin streamflow. Figure 9 shows the annual runoff generated in four snow regimes. HRUs were grouped into four blowing snow regimes (Rasouli et al., 2015), including sink and source, and intercepted and sheltered snow. These categories are based on topographic exposure and vegetation height (Pomeroy et al., 1997). Blowing snow sink HRUs include drift HRUs, riparian, and tall sage HRUs. The HRUs covered with short vegetation were grouped as source HRUs. The forested landscapes were divided into those that are subject to interception (coniferous fir) and those that are cleared or have negligible winter interception capacity (Deciduous aspen, Pomeroy et al., 2002). Runoff generated during ROS events varies with blowing snow regimes in different hydroclimatic phases (Figure 9). Forest landscapes with intercepted snow on canopies generate larger ROS runoff than other snow regimes in all six hydroclimatic phases (Figure 9a). The sheltered forest landscapes with minimal blowing wind generated the highest ROS runoff during phase three among all snow regimes, with 60% above normal (Figure 9a). This is likely due to the above-normal precipitation (206 mm, 21%) and below-normal winter air temperature (0.5 degC) during phase three, which prolonged the snow cover period by 16 days above normal (Table 3) and increased the frequency of the ROS events. In contrast to the sheltered HRUs, the blowing snow source HRUs showed the lowest (40% below normal) ROS runoff generation during phase two (Figure 9b). In phase two, annual precipitation was 163 mm (17%) below normal and the winter air temperature was 0.3degC warmer than the normal values (Table 3). Despite the high rainfall ratio in this phase, the modeled ROS runoff averaged for the entire basin was the lowest among the phases with 56 mm (31%) below normal (Table 3 and Figure 9). This is because of a short period of snow cover (21 days shorter than normal, Table 3) and the effect of a strong positive phase of NAO in hydroclimatic phase two (Figure 8). A mechanistic diagnosis on ROS runoff is critical as the mid-latitude basins are expected to experience warmer conditions and precipitation phase change from snow to rain in the future.

The observed runoff ratio, defined as the ratio of total annual runoff to total annual precipitation, varies between 13% above normal in phases one and three and 13% below normal in phase six (Table 3). Time series of the runoff ratio (Figure 8) are consistent with the values reported by Sridhar and Nayak (2010).

4.4 Synthesis of the hydrological linkage to climate teleconnection patterns in hydroclimatic phases

The time-averaged observed precipitation (snowfall and rainfall ratio), mean annual and winter air temperatures, observed streamflow, modeled ROS, observed peak SWE and observed snow cover duration in

Reynolds Mountain are reported in Table 3. The linkage of these variables in a small basin to regional climatic teleconnection patterns was synthesized for the six hydroclimatic phases as the following:

Phase one (1984-1986, cold and wet, high flow, negative phases of AO and SST). In this phase, the observed peak SWE and annual runoff were respectively 315 mm (63%) and 314 mm (57%) above normal, and the observed runoff ratio was up by 13% (Table 3). The observed mean annual air temperature was 0.6 oC below normal, and annual precipitation was 301 mm above normal, which makes this phase the coldest and wettest among the phases. The highest annual runoff and peak SWE were linked to strong negative phases of SST and AO (Figure 8). The high SWE accumulations and subsequent runoff generations were spatially restricted to areas with drifted snow and north facing HRUs (Figure 10). Runoff generated during ROS events were, however, quite low during phase one across Reynolds Mountain.

Phase two (1987-1994, dry, positive phases of NAO and AO) . The observed annual runoff and modeled ROS runoff were respectively 163 mm (30%) and 56 mm (31%) below normal (Table 3). A strong positive phase of NAO (Figure 8) locked the polar cold air in the Arctic region, leading to a slightly warmer and drier than normal winter in the study area in phase two, which restricted the generation of ROS runoff. As a result, this decreased the annual runoff. The spatial variations of modeled peak SWE and runoff were smaller than other wet phases, such as phase one (Figure 10).

Phase three (1995-1999, cold, high ROS runoff, negative AO, positive AAO). Mean annual air temperature was 0.6 oC below normal, and the annual ROS runoff was 57 mm (45%) above normal, the highest among the six phases (Table 3). Similar to phase one, high SWE accumulations and subsequent ROS runoff generations were spatially restricted to drift and north facing HRUs (Figure 10). The runoff depth was quite higher than peak SWE (Figure 10), indicating a substantial contribution from rainfall induced events to total runoff. Despite the similarity in snow, rain, and air temperature between this phase and phase one, a large difference is observed in ROS runoff. The only difference between the two phases is the type and phase of teleconnection patterns. Positive AAO is likely the main reason for high ROS runoff in this phase.

Phase four (2000-2003, warm, positive PNA). The annual and winter air temperatures were 0.7 degC and 0.5 degC above normal, respectively, causing this phase to be the warmest among the six phases with near-freezing winter temperatures (Table 3). Such hydrological responses suggested that Reynolds Mountain is very sensitive to changes in winter air temperature and warming of 0.5 oC can shift winter temperatures from below-freezing to above-freezing conditions, resulting in reduction of the ROS runoff by 9% below the normal. A relatively low flow condition in this phase is associated with the positive phase of PNA.

Phase five (2004-2011, normal, negative NAO, positive PNA) . Similar to phase three, the runoff generated from ROS events is high in this phase (36 mm (20%) above normal, Table 3), which is the second largest contribution to annual runoff among the six phases. The runoff amounts are higher than peak SWEs across the basin, indicating the substantial contribution of rainfall to total annual runoff (Figure 10). Positive PNA partly moderated the effect of negative NAO on air temperature and precipitation. It, however, was not enough to offset the effect of the negative NAO on runoff, and as a result, a slight increase in annual runoff and a relatively large increase in the ROS runoff were observed in this phase.

Phase six (2012-2014, dry, low flow, low runoff ratio, positive NAO, negative PNA) . This phase represents an extreme hydroclimatic condition. The observed annual precipitation was 194 mm (20%) below normal and the observed mean annual air temperature was 0.5 oC above normal. Warm and dry conditions caused observed peak SWE to drop 275 mm (55%) below normal, snow cover season to shorten 26 days below normal, and observed annual runoff to drop 234 mm (43%). The NAO and PNA phases are opposite of those in phase five, and as a result, there is an opposite response of the basin to phase change. The radical changes relative to phase five is associated with positive NAO, which led to dry, low snow, and low flow conditions. This clearly explains the important role of the phase of the climate teleconnection patterns in altering hydrological conditions in small basins.

DISCUSSION

Through linking hydrological fluxes at local scales to regional climatic teleconnection patterns beyond seasonal variations, we can better understand local hydrological processes across multiple years (Prein et al., 2015) and the nature of regional climate and hydrological extremes (Langendijk et al., 2019). Regional climatic patterns can explain nonlinear hydrological behaviors. For example, the hydroclimatic phases one and three in this study had similar annual air temperature and precipitation (<10% difference (Table 3)). Snow and ROS runoff, however, showed substantially different responses to variations of air temperature and precipitation. The observed peak SWE was 63% above normal in phase one and only 24% above normal in phase three. The modeled ROS runoff was 7% below normal in phase one, while it was 45% above normal in phase three (Table 3). Phase one was influenced by negative SST with La Nino events over 1984–1986, while positive AAO influenced phase three. Similar local hydrology and different climate teleconnection pattern (negative SST in phase one and negative AAO in phase three) explained a 52% difference in the modeled ROS runoff (Table 3). The same but opposite-sign teleconnections in phases five and six resulted in different snow and runoff conditions, wet in phase five and dry in phase six. This suggests that there is a strong linkage between teleconnection patterns and local hydrological regimes despite a scale mismatch. The different ROS runoff in phases one and three and the snow and runoff regimes in phases five and six highlighted the role of climate teleconnection patterns in dictating hydrological conditions at local scales. This is consistent with the findings of Whitfield (2001), which showed that small variations in climatic patterns can lead to large hydrological responses. Bonsal and Shabbar (2008) reported that low flow events in western Canada are associated with positive phases of the PNA pattern. The positive NAO, however, is more influential than the positive PNA pattern in decreasing the annual runoff and ROS runoff in Reynolds Mountain (phases two and six, Table 3).

The modeled ROS runoff had large temporal and spatial variations (Figure 9). High variability of ROS runoff implied that not only the regional climate teleconnections affected the local scale hydrology, but also vegetation heterogeneity played an important role. The sheltered forest landscapes with minimal blowing wind generated the highest ROS runoff during phase three (Figure 9a), while the blowing snow source HRUs showed the lowest ROS runoff in phase two. The above-normal precipitation (206 mm, 21%) and the below-normal winter air temperature (0.5 degC) during phase three prolonged the snow cover period by 8 days above normal (Table 3) and increased the frequency of the ROS events in the sheltered forest landscapes. Annual precipitation was 163 mm (17%) below normal and the winter air temperature was 0.3 degC warmer than the normal values (Table 3) in phase two, which led to the lowest ROS runoff in blowing snow sources HRUs among the six phases (Table 3 and Figure 9). This is because of a short period of snow cover in the warm phase and snow transport out of the source HRUs by blowing wind. The frequent ROS events are correlated with the positive phase of SST and El-Nino events (McCabe et al., 2007). Consistently, the hydroclimatic conditions in phase one with a negative SST (Figure 9) and La Nino events showed less frequent events by decreasing ROS runoff by 7% below normal (Table 3). A strong positive NAO in the hydroclimatic phases two and six (Figure 8) affected the interannual variability of snow cover (Derksen et al. 2008; Ge & Gong 2009; Bao et al. 2011) and locked the polar cold air in the Arctic region (Francis & Vavrus, 2012; Cohen et al., 2014), leading to a warmer, drier, and shorter than normal winter in the study area. Warm and dry conditions restricted the generation of ROS runoff, especially in HRUs with short vegetation (blowing snow source HRUs in Figure 9b). Therefore, positive NAO and AAO have more pronounced effects on ROS runoff than negative SST or positive PNA pattern. The positive NAO decreased the ROS runoff by 26% below normal, while the positive AAO increased the ROS runoff by 45% above normal (Table 3). A strong negative correlation between AAO and rainfall ratio (0.70, Figure 6a) indirectly showed the effect of AAO on the magnitude of ROS runoff by changing precipitation phase from snowfall to rainfall.

Despite a small effect of the negative SST on ROS runoff, it had the largest effect on annual peak SWE and runoff increase in Reynolds Mountain and it elevated the observed peak SWE and annual runoff by 63% and 57% above normal, respectively (phase one, Table 3). On the other hand, the positive NAO had the largest impact on snow and runoff drop and it decreased the observed peak SWE and annual runoff by 55% and

43%, respectively (phase six, Table 3), and the modeled ROS runoff by 31% (phase two). A high correlation between ROS runoff and NAO (Figure 6d) explained their potential relation.

The runoff generations in drift and north facing HRUs are sensitive to a wet climate with warm air temperatures (Figure 10). The modeled peak SWE is almost similar to a modeled runoff in these HRUs during dry phases (e.g., phase two) while under wet conditions (e.g., phase one) annual runoff is greater than peak SWE. The spatial variability of runoff under low flow conditions is very similar to that in the low ROS conditions (phase two and six in Figure 10). The highest annual runoff in Reynolds Mountain occurred when rainfall ratio was near the long term average and mean annual air temperature was 0.6 oC cooler than the average (phase one, Table 3). Under cold air temperatures, snowpack is usually deep and sustains the baseflows in summer, which may increase the annual runoff. Under warm air temperatures, however, we may not expect an increase in annual runoff (i.e., phase six) as both rainfall proportion of precipitation and ET will increase, which may cancel each other out (Rasouli, 2017; Rasouli et al., 2019a).

As the detected hydroclimatic phases are temporally evolving, they can be applied in short and medium range hydrological predictions. For instance, based on the distance of the present-year precipitation from the long term average (Figure 7) and because of a climatological persistence, it is likely that annual precipitation will be below normal for the following year after the sixth phase in Reynolds Mountain. Dutta and Maity (2018) found that a temporally evolving hydroclimatic teleconnection can improve the predictability of the monsoon rainfall at local scales. The application of climate variability patterns as an input to machine-learning methods has been shown to be skillful in improving short-term (Rasouli, Hsieh, & Cannon, 2012) and long-term (Rasouli, Nasri, Soleymani, Mahmood, Hori, & Torabi Haghighi, 2020) streamflow forecasts. A numerical representation of governing hydrological processes by a physically based model can help simulate and forecast the hydrological processes in the present and future climates under different phases of climate variability patterns such as AO (Thompson & Wallace, 1998), NAO (Walker & Bliss, 1932), AAO (Thompson & Wallace, 2000), SST in the Nino 3.4 region (Trenberth, 1997), and PNA, (Blackmon, Lee, Wallace, & Hsu, 1984).

The uncertainty in modeling the high flows using the CRHM model and accurate delineation of the hydroclimatic phases due to occasional overlapping of the positive and negative phases of different teleconnection patterns are the main limitations of this study and should be taken into account when interpreting the results.

CONCLUSIONS

In this study, we used a singular spectrum analysis and a physically based cold region hydrological model to characterize major hydroclimatic phases over 31 years at a mid-latitude headwater basin in Idaho, USA. Long data records in the basin and a spatially distributed lidar snow depth dataset provided foundational information for understanding both spatial and temporal hydroclimatic variations. The main findings of this research include:

1. Concomitant negative AO and SST in Nino 3.4 regions of the Equatorial Pacific Ocean resulted in extremely wet conditions with observed peak SWE of 315 mm (63%) above normal. The snow cover period was also extended by almost one month, leading to a 314 mm (57%) increase in observed annual runoff and a 13% increase in runoff ratio relative to long-term averages.
2. Concomitant negative PNA pattern and positive NAO resulted in extremely dry conditions with observed peak SWE being 275 mm (55%) below normal. The snow cover period was shortened by almost one month, leading to a 234 mm (43%) decrease in observed annual runoff and a 13% decrease in runoff ratio relative to long-term averages.
3. A positive phase of North Atlantic Oscillation (NAO) is more influential than a positive phase of the Pacific North American (PNA) pattern on the observed annual runoff and the modeled rain on snow runoff in the study area. A switch in the phase of the teleconnection patterns of NAO and PNA in

2012 was concomitant with a transition from wet to dry conditions in the basin.

4. Snowmelt and runoff generated during ROS events can account for up to one-third of the annual runoff. The areas of high snow accumulations (taller vegetation, north facing and steeper slope, and topographic depressions) produced more considerable runoff during ROS events. High ROS runoff is associated with positive AAO with high moisture transport from southern and equatorial latitudes and negative AO with cold air transport from the northern latitudes to the study area.

Linking hydrological variability in a small headwater basin to regional climatic patterns in this study can be used to improve forecast skills and further develop our understanding of land-atmosphere feedbacks. The warm and dry phases with multiple year durations (e.g., phase six) identified in this study can be extended to diagnose the effects of potential future warm and dry conditions on water flow and storage at local scales and develop appropriate water security plans in regions that depend on snowmelt water from high elevations.

ACKNOWLEDGMENTS

We appreciate efforts and commitment to the long term collection of high quality records in Reynolds Creek Experimental Watershed by researchers and technicians in the US Agricultural Research Service. The research was funded by the NSF funded ND EPSCoR (NSF grant #IIA-135466) to THM and by the Canadian Natural Science and Engineering Research Council post-doctoral fellowship to KR. We would like to thank two anonymous reviewers for their constructive comments on an earler version of this paper.

Data Availability. The data that support the findings of this study are openly available from the anonymous ftp site ftp://ftp.nwrc.ars.usda.gov/publications/wrr/rme-25yr-data maintained by the USDA Agricultural Research Service, Northwest Watershed Research Center, in Boise, Idaho (Reba et al., 2011a). The data for climatic teleconnection patterns were downloaded from the National Oceanic and Atmospheric Administration Earth System Research Laboratory (NOAA) website (http://www.esrl.noaa.gov).

REFERENCES

Alexandrov, T., Bianconcini, S., Dagum, E. B., Maass, P., & McElroy, T. S. (2012). A review of some modern approaches to the problem of trend extraction. *Econometric Reviews* , 31(6), 593–624.

Armstrong, R. N., Pomeroy, J. W., & Martz, L. W. (2010). Estimating evaporation in a Prairie landscape under drought conditions.*Canadian Water Resources Journal, 35* (2), 173-186. doi:10.4296/cwrj3502173.

Ayers, H. (1959). Influence of soil profile and vegetation characteristics on net rainfall supply to runoff. In *Proceedings of Hydrology Symposium, 1* , 198-205.

Bao, Z., Kelly, R. & Wu, R. (2011). Variability of regional snow cover in spring over western Canada and its relationship to temperature and circulation anomalies. *International Journal of Climatology* , 31 (9), 1280–1294.

Blackmon, M. L., Lee, Y., Wallace, J. M., & Hsu, H. (1984). Time variation of 500 mb height fluctuations with long, intermediate and short time scales as deduced from lag-correlation statistics.*Journal of the Atmospheric Sciences, 41* , 981–991, https://doi.org/10.1175/1520-0469(1984)041<0981:TVOMHF>2.0.CO;2.

Bonsal, B. & Shabbar, A. (2008). Impacts of large-scale circulation variability on low streamflows over Canada: a review. *Canadian Water Resources Journal* , 33 (2), 137–154.

Brooks, R., & Corey, A. (1964). Hydraulics properties of porous media.*Hydrology Paper* , Colorado State University *(3)* , 1-29.

Carey, S. K., Quinton, W. L., & Goeller, N. T. (2007). Field and laboratory estimates of pore size properties and hydraulic characteristics for subarctic organic soils. *Hydrological Processes, 21* (19), 2560–2571.

Chen, X., Kumar, M., Wang, R., Winstral, A., & Marks, D. (2016). Assessment of the Timing of Daily Peak Streamflow during the Melt Season in a Snow-Dominated Watershed. *Journal of Hydrometeorology,17* (8), 2225-2244.

Clark, C., 1945. Storage and the unit hydrograph. *Transactions of the American Society of Civil Engineers* , *110* (1), 1419-1446.

Cohen, J., Screen, J. A., Furtado, J. C., Barlow, M., Whittleston, D., Coumou, D., Francis, J., Dethloff, K., Entekhabi, D., Overland, J., Jones, J. (2014). Recent Arctic amplification and extreme mid-latitude weather. *Nature Geoscience* , 7(9), 627.

Daubechies, I. (1992). Ten lectures on wavelets, 61, Siam.

DeBeer, C. M., & Pomeroy, J. W. (2010). Simulation of the snowmelt runoff contributing area in a small alpine basin. *Hydrology and Earth System Sciences, 14* (7), p.1205.

Derksen, C., Brown, R., MacKay, M. (2008). Mackenzie basin snow cover: Variability and trends from conventional data, satellite remote sensing, and Canadian regional climate model simulations. In Cold Region Atmospheric and Hydrologic Studies. The Mackenzie GEWEX Experience, 213–239, Springer.

Dornes, P. F., Pomeroy, J. W., Pietroniro, A., Carey, S. K., & Quinton, W. L. (2008). Influence of landscape aggregation in modeling snow-cover ablation and snowmelt runoff in a sub-arctic mountainous environment.*Hydrological Sciences Journal, 53* (4):725-740.

Dutta, R., & Maity, R. (2018). Temporal evolution of hydroclimatic teleconnection and a time-varying model for long-lead prediction of Indian summer monsoon rainfall. *Scientific Reports* , *8* (1), p.10778.

Ellis, C. R., & Pomeroy, J. W. (2007). Estimating sub-canopy shortwave irradiance to melting snow on forested slopes. *Hydrological Processes, 21* (19), 2581-2593.

Ellis, C., Pomeroy, J. W., Brown, T., & MacDonald, J. (2010). Simulation of snow accumulation and melt in needleleaf forest environments. *Hydrology and Earth System Sciences, 14* (6), 925-940.

Ellis, C., Pomeroy, J. W., & Link, T. (2013). Modeling increases in snowmelt yield and desynchronization resulting from forest gap-thinning treatments in a northern mountain headwater basin. *Water Resources Research, 49* (2), 936-949.

Fan, Y., Clark, M., Lawrence, D. M., Swenson, S., Band, L. E., Brantley, S. L.,. . . , Yamazaki, D. (2019). Hillslope Hydrology in Global Change Research and Earth System Modeling, *Water Resources Research* , *55* , 1737–1772. https://doi.org/10.1029/2018WR023903.

Fang, X., Pomeroy, J. W., Ellis, C., MacDonald, M., DeBeer, C., & Brown, T. (2013). Multi-variable evaluation of hydrological model predictions for a headwater basin in the Canadian Rocky Mountains.*Hydrology and Earth System Sciences, 17* (4), 1635–1659.

Flerchinger, G. N., Reba, M. L., & Marks, D. (2012). Measurement of surface energy fluxes from two rangeland sites and comparison with a multilayer canopy model. *Journal of Hydrometeorology,13* (3), 1038–1051.

Fowler, H., Blenkinsop, S., & Tebaldi, C. (2007). Linking climate change modelling to impacts studies: recent advances in downscaling techniques for hydrological modelling. *International Journal of Climatology, 27* (12), 1547–1578.

Francis, J.A., & Vavrus, S. J. (2012). Evidence linking Arctic amplification to extreme weather in mid-latitudes. *Geophysical Research Letters* , 39(6).

Garnier, B., & Ohmura, A. (1970). The evaluation of surface variations in solar radiation income. *Solar Energy, 13* (1), 21-34.

Ge, Y., & Gong, G. (2009). North American snow depth and climate teleconnection patterns. *Journal of Climate,* 22(2), 217–233.

Gong, D., & Wang, S. (1999). Definition of Antarctic oscillation index.*Geophysical research letters* , 26(4), 459-462.

Granger, R. J., & Gray, D. (1989). Evaporation from natural nonsaturated surfaces. *Journal of Hydrology, 111* (1), 21-29.

Gray, D., Toth, B., Zhao, L., Pomeroy, J. W., & Granger, R. (2001). Estimating areal snowmelt infiltration into frozen soils.*Hydrological Processes, 15* (16), 3095-3111.

Harder, P., & Pomeroy, J. W. (2013). Estimating precipitation phase using a psychrometric energy balance method. *Hydrological Processes* , *27* (13), 1901-1914.

Huang, N. E., Shen, Z., Long, S. R., Wu, M. C., Shih, H. H., Zheng, Q., Yen, N.-C., Tung, C. C., & Liu, H. H. (1998). The empirical mode decomposition and the Hilbert spectrum for nonlinear and non-stationary time series analysis. *Proceedings of the Royal Society of London. Series A: Mathematical, Physical and Engineering Sciences,* 454(1971), 903–995.

Hurrell, J.W., Kushnir, Y., Ottersen, G. and Visbeck, M. (2003). An overview of the North Atlantic oscillation. *Geophysical Monograph-American Geophysical Union* , 134, pp.1-36.

Kumar, M., Wang, R., & Link, T. E. (2012). Effects of more extreme precipitation regimes on maximum seasonal snow water equivalent.*Geophysical Research Letters, 39* (20), DOI: 10.1029/2012GL052972.

Kumar, M., Marks, D., Dozier, J., Reba, M., & Winstral, A. (2013). Evaluation of distributed hydrologic impacts of temperature-index and energy-based snow models. *Advances in Water Resources, 56* , 77-89.

Hsieh, W. W. (2009). *Machine Learning Methods in the Environmental Sciences* . Cambridge University Press.

Langendijk, G., Aubry-Wake, C., Osman, M., Gulizia, C., Attig-Bahar, F., Behrens, E., Bertoncini, A., Hart, N., Indasi, V. S., Innocenti, S., van der Linden, E. C., Mamnun, N. , Rasouli, K., et al., (2019). Three ways forwards to improve regional information for extreme events: an early career perspective. *Frontiers in Environmental Science, 7* , 1-7.

Leavesley, G. H., Lichty, R., Thoutman, B., & Saindon, L. (1984).*Precipitation-runoff modeling system: User's manual, volume 83 of Water-resources Investigations* . US Geological Survey Colorado, CO. pp. 207.

Lehning, M., Grunewald, T. & Schirmer, M. (2011). Mountain snow distribution governed by an altitudinal gradient and terrain roughness.*Geophysical Research Letters* , *38* (19).

Li, D., Wrzesien, M. L., Durand, M., Adam, J., & Lettenmaier, D. P. (2017). How much runoff originates as snow in the western United States, and how will that change in the future?. *Geophysical Research Letters, 44* (12), 6163–6172.

Link, T. E., Flerchinger, G. N. Unsworth, M., & Marks, D. (2004). Simulation of water and energy fluxes in an old-growth seasonal temperate rain forest using the simultaneous heat and water (SHAW) model. *Journal of Hydrometeorology, 5* (3), 443–457.

Lopez-Moreno, J., Pomeroy, J. W., Revuelto, J., & Vicente-Serrano, S. (2013). Response of snow processes to climate change: spatial variability in a small basin in the Spanish Pyrenees. *Hydrological Processes, 27* (18), 2637-2650.

MacDonald, R. J., Byrne, J. M., Kienzle, S. W., & Larson, R. P. (2011). Assessing the potential impacts of climate change on mountain snowpack in the St. Mary River Watershed, Montana. *Journal of Hydrometeorology, 12* (2), 262-273.

Mahmood, T. H., Pomeroy, J. W., Wheater, H. S., Baulch, H. M. (2017). Hydrological responses to climatic variability in a cold agricultural region. *Hydrological Processes, 31* (4), 854-870.

Manning, A. H., Clark, J. F., Diaz, S. H., Rademacher, L. K., Earman, S., & Plummer, L. N. (2012). Evolution of groundwater age in a mountain watershed over a period of thirteen years. *Journal of Hydrology, 460* , 13–28.

Marks, D., & Winstral, A. (2001). Comparison of snow deposition, the snow cover energy balance, and snowmelt at two sites in a semiarid mountain basin. *Journal of Hydrometeorology, 2* (3), 213-227.

Marks, D., Kimball, J., Tingey, D., & Link, T. (1998). The sensitivity of snowmelt processes to climate conditions and forest cover during rain-on-snow: A case study of the 1996 Pacific Northwest flood.*Hydrological Processes, 12* , 1569-1587.

Marks, D., Link, T., Winstral, A., & Garen, D. (2001). Simulating snowmelt processes during rain-on-snow over a semi-arid mountain basin.*Annals of Glaciology, 32* , 195-202.

Marks, D., Winstral, A., Reba, M., Pomeroy, J. W., Kumar, M. (2013). An evaluation of methods for determining during-storm precipitation phase and the rain/snow transition elevation at the surface in a mountain basin. *Advances in Water Resources, 55* , 98-110.

McCabe, G. J., Clark, M. P., & Hay, L. E. (2007). Rain-on-snow events in the western United States. *Bulletin of the American Meteorological Society* , 88(3), 319-328.

McCartney, S. E., Carey, S. K., Pomeroy, J. W. (2006). Intra-basin variability of snowmelt water balance calculations in a subarctic catchment. Hydrological Processes 20(4), 1001-1016.

Mote, P. W., Hamlet, A. F., Clark, M. P., & Lettenmaier, D. P. (2005). Declining mountain snowpack in Western North America. *Bulletin of the American Meteorological Society* , *86* , 39-49.

Nayak, A. (2008). *The effect of climate change on the hydrology of a mountainous catchment in the western United States: A case study at Reynolds Creek, Idaho.* Utah State University, pp. 194.

Nayak, A., Marks, D., Chandler, D. G., & Seyfried, M. (2010). Long-term snow, climate, and streamflow trends at the Reynolds Creek Experimental Watershed, Owyhee Mountains, Idaho, United States. *Water Resources Research, 46* (6).

Nayak, A., Marks, D., Chandler, D. G., & Winstral, A. (2011). Modeling interannual variability in snow-cover development and melt for a semiarid mountain catchment. *Journal of Hydrologic Engineering, 17* (1), 74-84.

Newman, A. J., Clark, M. P., Winstral, A., Marks, D., & Seyfried, M. (2014). The use of similarity concepts to represent subgrid variability in land surface models: Case study in a snowmelt-dominated watershed.*Journal of Hydrometeorology, 15* (5), 1717-1738.

Oke, T. (1978). *Boundary Layer Climates* . Methuen, New York, pp. 372.

Overland, J. E., & Wang, M. (2010). Large-scale atmospheric circulation changes are associated with the recent loss of Arctic sea ice.*Tellus A* , 62(1), 1-9.

Plummer, L. N., Busenberg, E., Bohlke, J. K., Nelms, D. L., Michel, R. L., & Schlosser, P. (2001). Groundwater residence times in Shenandoah National Park, Blue Ridge Mountains, Virginia, USA: a multi-tracer approach. *Chemical Geology, 179* (1-4), 93–111.

Pomeroy, J. W., & Li, L. (2000). Prairie and Arctic areal snow cover mass balance using a blowing snow model. *Journal of Geophysical Research, 105* (D21), 26619-26634.

Pomeroy, J. W., Marsh, P., & Gray, D. M., (1997). Application of a distributed blowing snow model to the Arctic. Hydrological Processes 11(11), 1451–1464.

Pomeroy, J. W., Hedstrom, N., & Parviainen, J. (1999). The snow mass balance of Wolf Creek, Yukon: effects of snow sublimation and redistribution. Wolf Creek Research Basin–Hydrology, Ecology, Environment–Proceedings of a workshop held in Whitehorse, Yukon, (Eds: Pomeroy, J. W. and Granger R. J., 15–30.

Pomeroy, J. W., Gray, D. M., Hedstrom, N. R., & Janowicz, J. R. (2002). Prediction of seasonal snow accumulation in cold climate forests. Hydrological Processes, 16(18), 3543–3558.

Pomeroy, J. W., Toth, B., Granger, R., Hedstrom, N., & Essery, R. (2003). Variation in surface energetics during snowmelt in a subarctic mountain catchment. *Journal of Hydrometeorology, 4* (4), 702–719.

Pomeroy, J. W., Bewley, D. S., Essery, R. L. H., Hedstrom, N. R., Link, T., Granger, R. J., Sicart, J. E., Ellis, C. R., & Janowicz J. R. (2006). Shrub tundra snowmelt. *Hydrological Processes, 20* (4), 923–941, DOI: 10.1002/hyp.6124.

Pomeroy, J. W., Gray, D., Brown, T., Hedstrom, N., Quinton, W., Granger, R., & Carey, S. (2007). The cold regions hydrological model: a platform for basing process representation and model structure on physical evidence. *Hydrological Processes, 21* (19), 2650–2667.

Pomeroy, J. W., Fang, X., & Rasouli, K. (2015). Sensitivity of snow processes to warming in the Canadian Rockies. *Proceeding of the 72nd Eastern Snow Conference* , Sherbrooke, Quebec, Canada, 22–33.

Prein, A. F., Langhans, W., Fosser, G., Ferrone, A., Ban, N., Goergen, K., Keller, M., Tolle, M., Gutjahr, O., Feser, F. and Brisson, E. (2015). A review on regional convection-permitting climate modeling: Demonstrations, prospects, and challenges. *Reviews of Geophysics, 53* (2), 323-361.

Quinton, W. L., & Carey, S. K. (2008). Towards an energy-based runoff generation theory for tundra landscapes. *Hydrological Processes, 22* (23), 4649-4653.

Rasouli, K. (2017). *Sensitivity analysis of mountain hydrology to changing climate.* Ph.D. thesis, pp. 251, University of Saskatchewan, Saskatoon, Canada.

Rasouli, K., Hsieh, W. W., & Cannon, A. J. (2012). Daily streamflow forecasting by machine learning methods with weather and climate inputs.*Journal of Hydrology, 414* , 284-293.

Rasouli, K., Pomeroy, J. W., Janowicz, J. R., Carey, S. K., & Williams, T. J. (2014). Hydrological sensitivity of a northern mountain basin to climate change. *Hydrological Processes, 28* (14), 4191-4208.

Rasouli, K., Pomeroy, J. W., & Marks, D. G. (2015). Snowpack sensitivity to perturbed climate in a cool mid-latitude mountain catchment. *Hydrological Processes, 29* (18), 3925-3940.

Rasouli K., Pomeroy, J. W., & Whitfield, P. H. (2019a). Hydrological responses of headwater basins to perturbed climate in North American Cordillera. *Journal of Hydrometeorology, 20* , 863-882, DOI: 10.1175/JHM-D-18-0166.1.

Rasouli K., Pomeroy, J. W., & Whitfield, P. H. (2019b). Are the effects of vegetation and soil changes as important as climate change impacts on hydrological processes? *Hydrology and Earth System Sciences* , 23, 4933–4954, DOI: 10.5194/hess-23-4933-2019.

Rasouli K., Nasri B., Soleymani A., Mahmood T., Hori M., Torabi Haghighi A. (2020). Forecast of streamflows to the Arctic Ocean by a Bayesian neural network model with snowcover and climate inputs. *Hydrology Research* , 51 (3), 541–561, nh2020164, DOI: 10.2166/nh.2020.164.

Reba, M. L., Marks, D., Seyfried, M., Winstral, A., Kumar, M., & Flerchinger, G., (2011a). A long-term data set for hydrologic modeling in a snow-dominated mountain catchment. *Water Resources Research, 47* (7).

Reba, M. L., Marks, D., Winstral, A., Link, T. E., & Kumar, M. (2011b). Sensitivity of the snowcover energetics in a mountain basin to variations in climate. *Hydrological Processes, 25* (21), 3312-3321.

Reba, M. L., Pomeroy, J. W., Marks, D., & Link, T. E. (2012). Estimating surface sublimation losses from snowpacks in a mountain catchment using eddy covariance and turbulent transfer calculations.*Hydrological Processes, 26* (24), 3699–3711.

Reba, M. L., Marks, D., Link, T. E., Pomeroy, J. W., & Winstral, A. (2014). Sensitivity of model parameterizations for simulated latent heat flux at the snow surface for complex mountain sites. *Hydrological Processes, 28* (3), 868–881.

Seyfried, M. S., Grant, L. E., Marks, D., Winstral, A., & McNamara, J. (2009). Simulated soil water storage effects on streamflow generation in a mountainous snowmelt environment, Idaho, USA. *Hydrological. Processes, 23* (6), 858-873.

Shrestha, R., & Glenn, N. F. (2016). 2007 Lidar-Derived Digital Elevation Model, Canopy Height Model and Vegetation Cover Model Data Sets for Reynolds Creek Experimental Watershed, Southwestern Idaho [Data set]. Retrieved from http://doi.org/10.18122/B27C77.

Sicart, J.-E., Pomeroy, J. W., Essery, R., & Bewley, D. (2006). Incoming longwave radiation to melting snow: observations, sensitivity and estimation in northern environments. *Hydrological Processes, 20* (17), 3697-3708.

Sridhar, V., & Nayak, A. (2010). Implications of climate-driven variability and trends for the hydrologic assessment of the Reynolds Creek Experimental Watershed, Idaho. *Journal of Hydrology, 385* (1-4), 183-202.

Tennant, C. J., Harpold, A. A., Lohse, K. A., Godsey, S. E., Crosby, B. T., Larsen, L. G., Brooks, P. D., Van Kirk, R. W., & Glenn, N. F. (2017). Regional sensitivities of seasonal snowpack to elevation, aspect, and vegetation cover in western North America. *Water Resources Resesearch, 53* (8), 6908-6926. doi:10.1002/2016WR019374,

Thompson, D. W. J., & Wallace, J. M. (1998). The Arctic oscillation signature in wintertime geopotential height and temperature fields.*Geophysical Research Letters,* 25, 1297–1300.

Thompson, D. W. J., & Wallace J. M. (2000). Annular modes in the extratropical circulation. Part I: month-to-month variability.*Journal of Climate* , *13* , 1000–1016.

Trenberth, K. E. (1997). The definition of el nino. *Bulletin of the American Meteorological Society* , *78* (12), pp.2771-2778.

Verseghy, D. L. (1991). Class-a Canadian land surface scheme for GCMs. I. Soil model. *International Journal of Climatology,11* (2), 111-133.

Walker, G. T., & Bliss, E. W. (1932). *World weather.Memoirs of the Royal Meteorological Society, 4* , 53–84.

Wang, R., Kumar, M., & Marks, D. (2013). Anomalous trend in soil evaporation in a semi-arid, snow-dominated watershed. *Advances in Water Resources* , *57* , 32-40.

Whitfield, P. H. (2001). Linked hydrologic and climate variations in British Columbia and Yukon. *Environmental Monitoring and Assessment* , *67* (1-2), 217-238.

Whitfield, P. H., Moore, R. D., Fleming, S.W., & Zawadzki, A. (2010). Pacific Decadal Oscillation and the hydroclimatology of western Canada—Review and prospects. *Canadian Water Resources Journal ,35* (1), 1-28.

Williams, T. J., Pomeroy, J. W., Janowicz, J. R., Carey, S. K., Rasouli, K., & Quinton. W. L. (2015). A radiative–conductive–convective approach to calculate thaw season ground surface temperatures for modelling frost table dynamics. *Hydrological Processes ,29* (18), 3954–3965.

Winstral, A., & Marks, D. (2014). Long-term snow distribution observations in a mountain catchment: Assessing variability, time stability, and the representativeness of an index site. *Water Resources Research, 50* (1), 293–305.

Winstral, A., Marks, D., & Gurney, R. (2013). Simulating wind-affected snow accumulations at catchment to basin scales. *Advances in Water Resources, 55* , 64–79.

Figure Captions:

FIGURE 1 Location of the study area: (a) Reynolds Creek Experimental Watershed (RCEW) in Idaho, USA. (b) Reynolds Mountain within RCEW. (c) Digital Elevation Model (DEM) of Reynolds Mountain.

FIGURE 2 Physiographic characteristics of the Reynolds Mountain basin including (a) elevation range, (b) slope, and (c) aspect.

FIGURE 3 Hydrologic response units (HRUs) used for hydrological modeling in Reynolds Mountain (22 HRUs) classified based on vegetation type and topographic characteristics.

FIGURE 4 Evaluation of the modeled snow water equivalent (SWE) against observations at the snow pillow site in Reynolds Mountain during 1984-2008. The blue line represents observed SWE, the red line represents modeled SWE, and the black line shows cumulative snowfall in respective winters.

FIGURE 5 Comparison between observed lidar snow depth and simulated snow depth in meters.

FIGURE 6 Correlation between regional climatic teleconnections and hydrological fluxes at local scales, includingt_a : mean annual air temperature,t_w : mean air temperature in winter, P : mean annual precipitation, Rain: mean annual rainfall,$Rain_{ratio}$: proportional ratio of annual rainfall to total solid and liquid annual precipitation; Snow: total annual snowfall, Runoff: total annual runoff from snowmelt and rainfall,R_{ratio} : proportional ratio of annual runoff to total solid and liquid annual precipitation, $\mathrm{R}_{\mathrm{ROS}}$: runoff generated during rain-on-snow events, SWE : annual peak snow water equivalent, SWE_{date} : timing of the peak snow water equivalent. Points at y = 0 indicate that the highest correlations are between the same year teleconnections and hydrological fluxes. Points below zero indicate a one-year lagged correlation meaning that the hydrological flux is affected by teleconnections in the preceding year. Points above zero indicate that the hydrological flux is affected by teleconnections in the following year.

FIGURE 7 Identification of six hydroclimatic phases based on the decomposed time series of daily precipitation over 1983-2014 and first eigenvector of the singular spectrum analysis (SSA), representing an intermediate (multiple year) frequency of the precipitation variations.

FIGURE 8 Anomalies of observed precipitation, winter air temperature, modeled rainfall ratio, observed runoff ratio and the selected teleconnection indices over the period of 1993-2014. These indices are Antarctic Oscillation (AAO), Sea Surface Temperature (SST) anomalies in the Nino 3.4 region of Equatorial Pacific Ocean, Arctic Oscillation (AO), North Atlantic Oscillation (NAO), and Pacific North American index (PNA). Vertical lines separate the six hydroclimatic phases.

FIGURE 9 (a) Total mean annual runoff generated during rain on snow (ROS) events based on snow cover and rainfall occurrence and (b) its anomalies relative to the long-term averages in four blowing snow regimes, including source, sink, sheltered forest, and forest with intercepted snow on the canopy in Reynolds Mountain in different hydroclimatic phases. Heterogeneity of snow cover due to topography and redistribution of snow by blowing wind affects the runoff generated during rain on snow events. Snow transport to sinks and topographic depressions with drifted snow can intensify snowmelt in spring and early summer when the likelihood of precipitation to fall as rain is high.

FIGURE 10 Distributed modeled peak SWE and annual runoff for each of the six hydroclimatic phases: Phase one – high flow under negative phases of AO and SST; Phase two – warm and dry under positive NAO and AO; Phase three – cold and high rain on snow runoff under negative AO and positive AAO; Phase four – warm conditions under positive PNA; Phase five – normal conditions under positive PNA pattern and negative NAO; and Phase six – warm and dry under negative PNA and positive NAO.

Hosted file

`Table1.docx` available at https://authorea.com/users/336824/articles/462510-linking-hydrological-variations-at-local-scales-to-regional-climatic-teleconnection-patterns

Hosted file

`Table2.docx` available at https://authorea.com/users/336824/articles/462510-linking-hydrological-variations-at-local-scales-to-regional-climatic-teleconnection-patterns

Hosted file

Table3.docx available at https://authorea.com/users/336824/articles/462510-linking-hydrological-variations-at-local-scales-to-regional-climatic-teleconnection-patterns

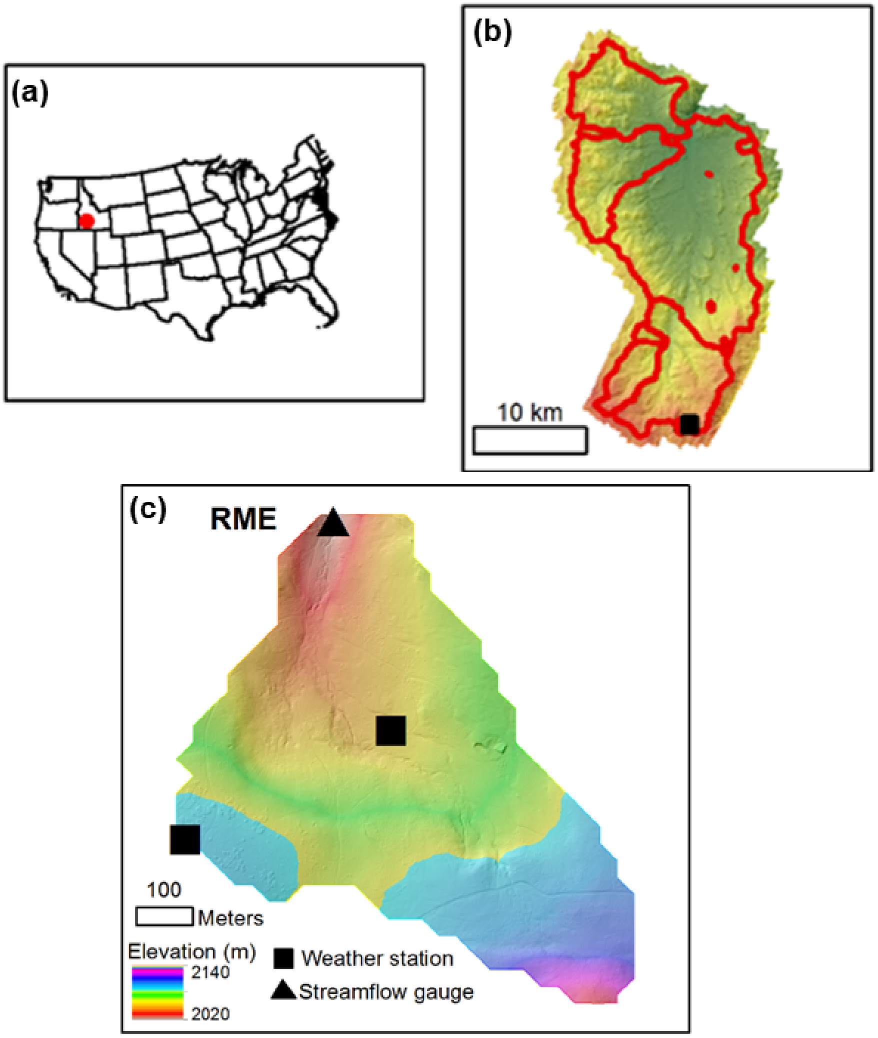

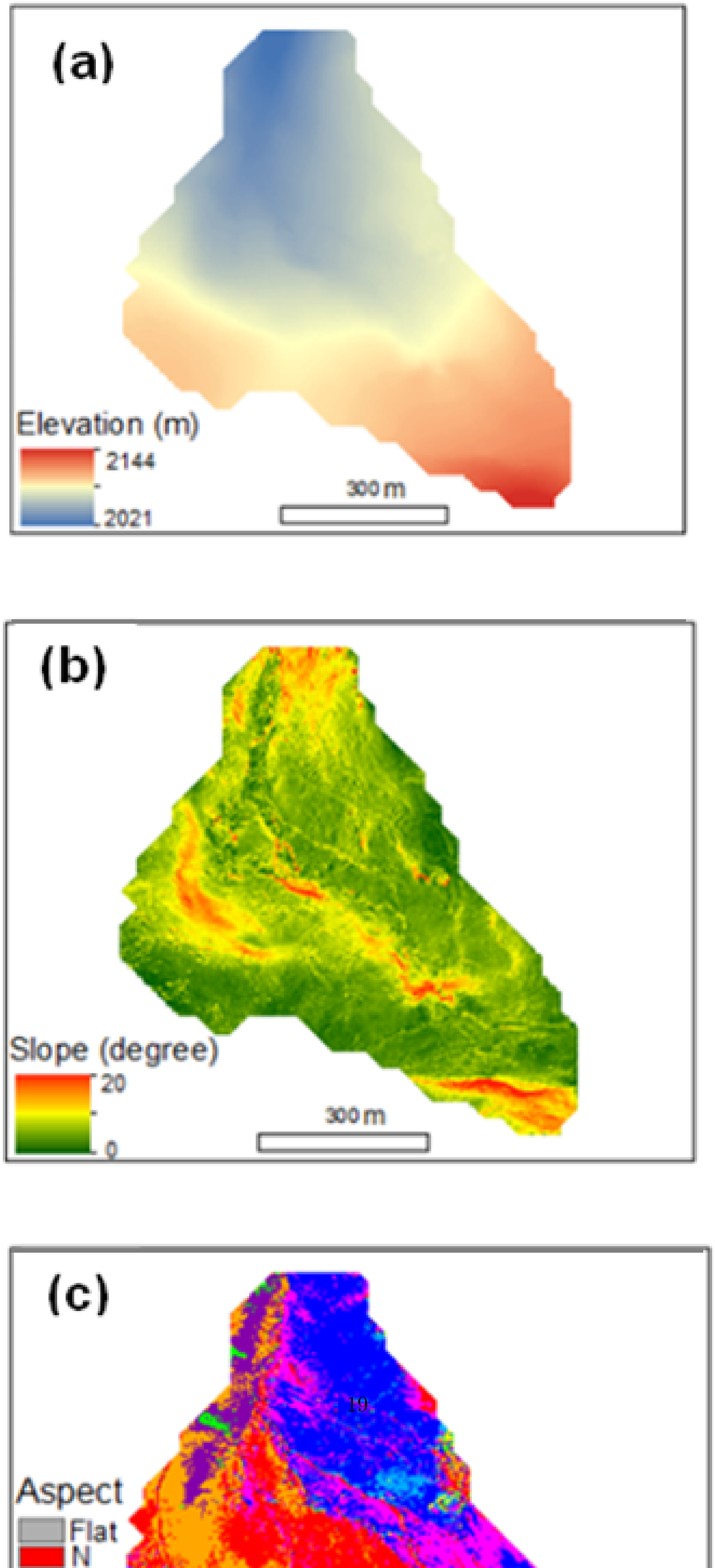
(a)
Elevation (m)
2144
2021
300 m
(b)
Slope (degree)
20
0
300 m
(c)
Aspect
Flat
N

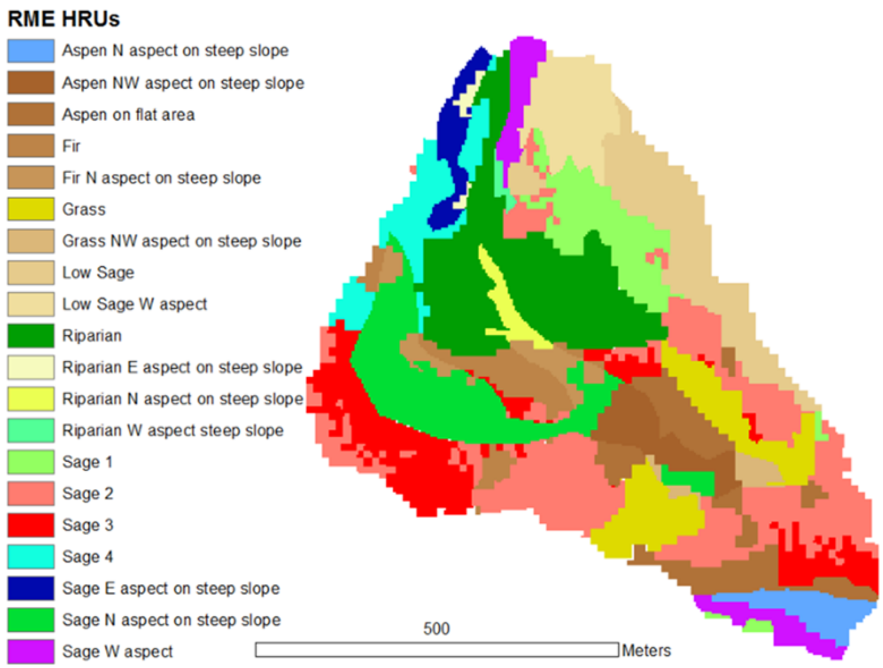
RME HRUs
Aspen N aspect on steep slope
Aspen NW aspect on steep slope
Aspen on flat area
Fir
Fir N aspect on steep slope
Grass
Grass NW aspect on steep slope
Low Sage
Low Sage W aspect
Riparian
Riparian E aspect on steep slope
Riparian N aspect on steep slope
Riparian W aspect steep slope
Sage 1
Sage 2
Sage 3
Sage 4
Sage E aspect on steep slope
Sage N aspect on steep slope
Sage W aspect
500
Meters

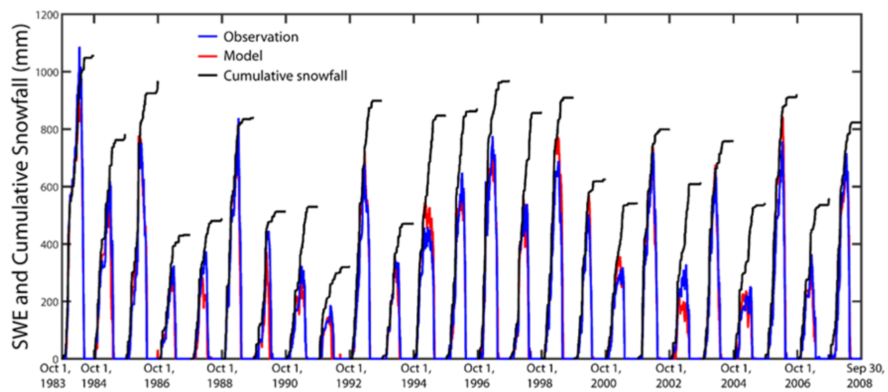
SWE and Cumulative Snowfall (mm)
1200
1000
800
600
400
200
0
Observation
Model
Cumulative snowfall
Oct 1, 1983
Oct 1, 1984
Oct 1, 1986
Oct 1, 1988
Oct 1, 1990
Oct 1, 1992
Oct 1, 1994
Oct 1, 1996
Oct 1, 1998
Oct 1, 2000
Oct 1, 2002
Oct 1, 2004
Oct 1, 2006
Sep 30, 2008

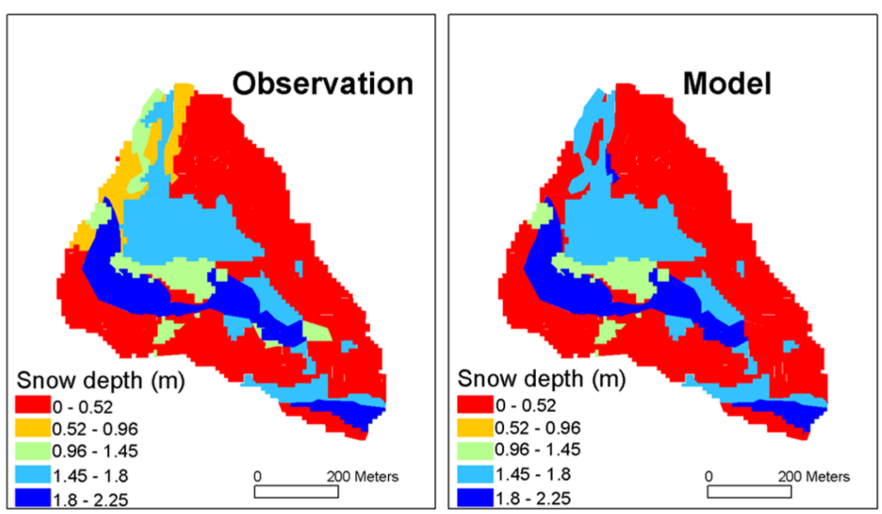
Observation
Snow depth (m)
0 - 0.52
0.52 - 0.96
0.96 - 1.45
1.45 - 1.8
1.8 - 2.25
0
200 Meters
Model
Snow depth (m)
0 - 0.52
0.52 - 0.96
0.96 - 1.45
1.45 - 1.8
1.8 - 2.25
0
200 Meters

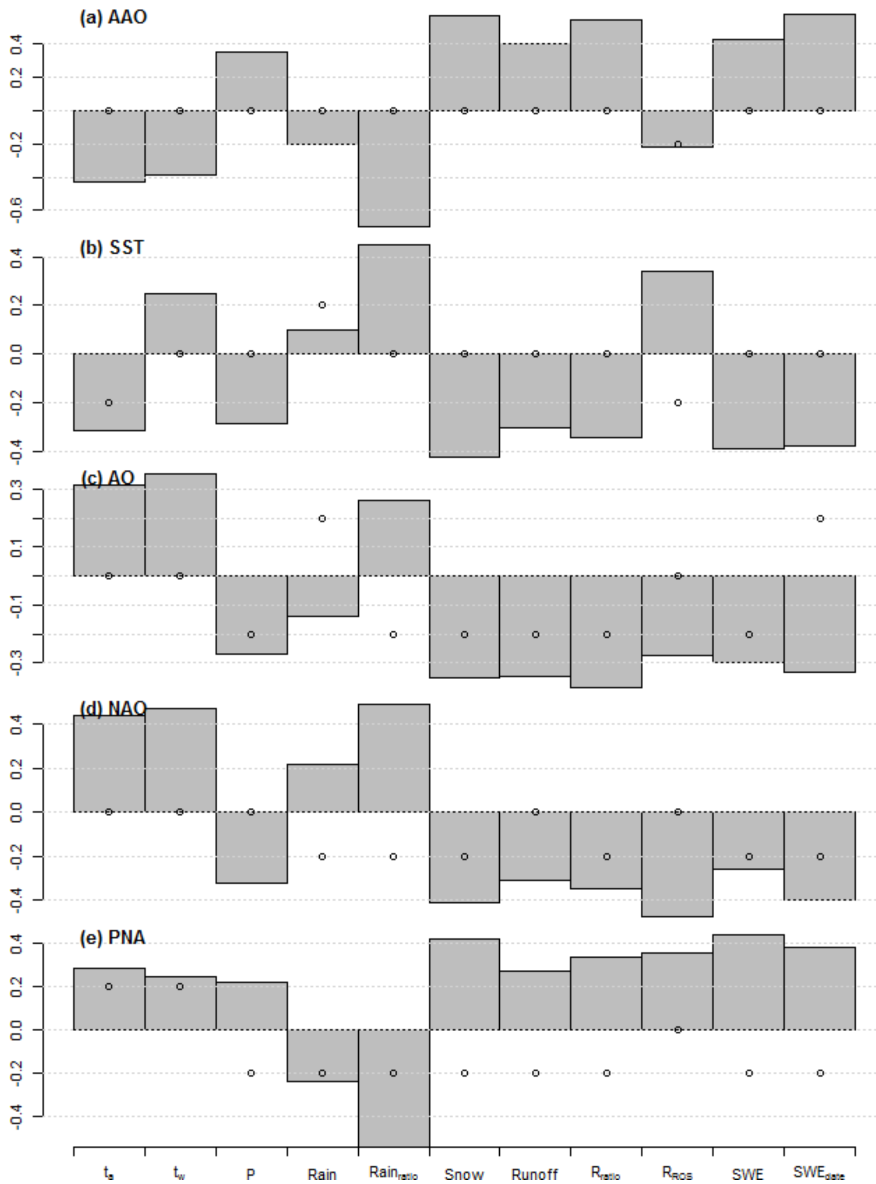

(a) AAO
(b) SST
(c) AO
(d) NAO
(e) PNA
t_s
t_w
P
Rain
$Rain_{ratio}$
Snow
Runoff
R_{ratio}
R_{ROS}
SWE
SWE_{date}

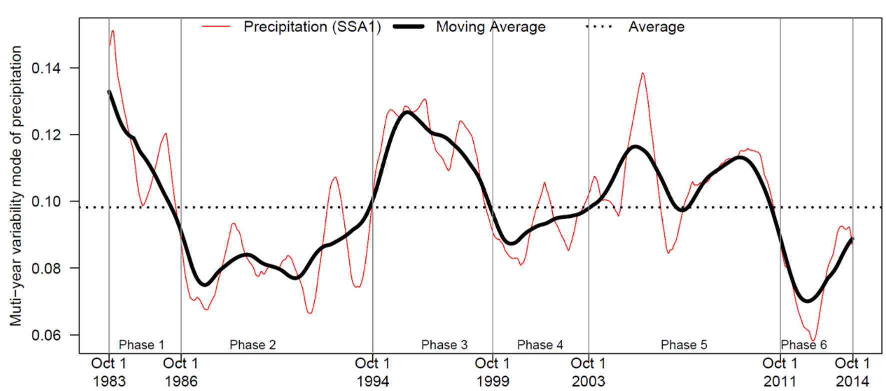

Precipitation (SSA1)
Moving Average
Average
Muti−year variability mode of precipitation
Phase 1
Phase 2
Phase 3
Phase 4
Phase 5
Phase 6
Oct 1 1983
Oct 1 1986
Oct 1 1994
Oct 1 1999
Oct 1 2003
Oct 1 2011
Oct 1 2014

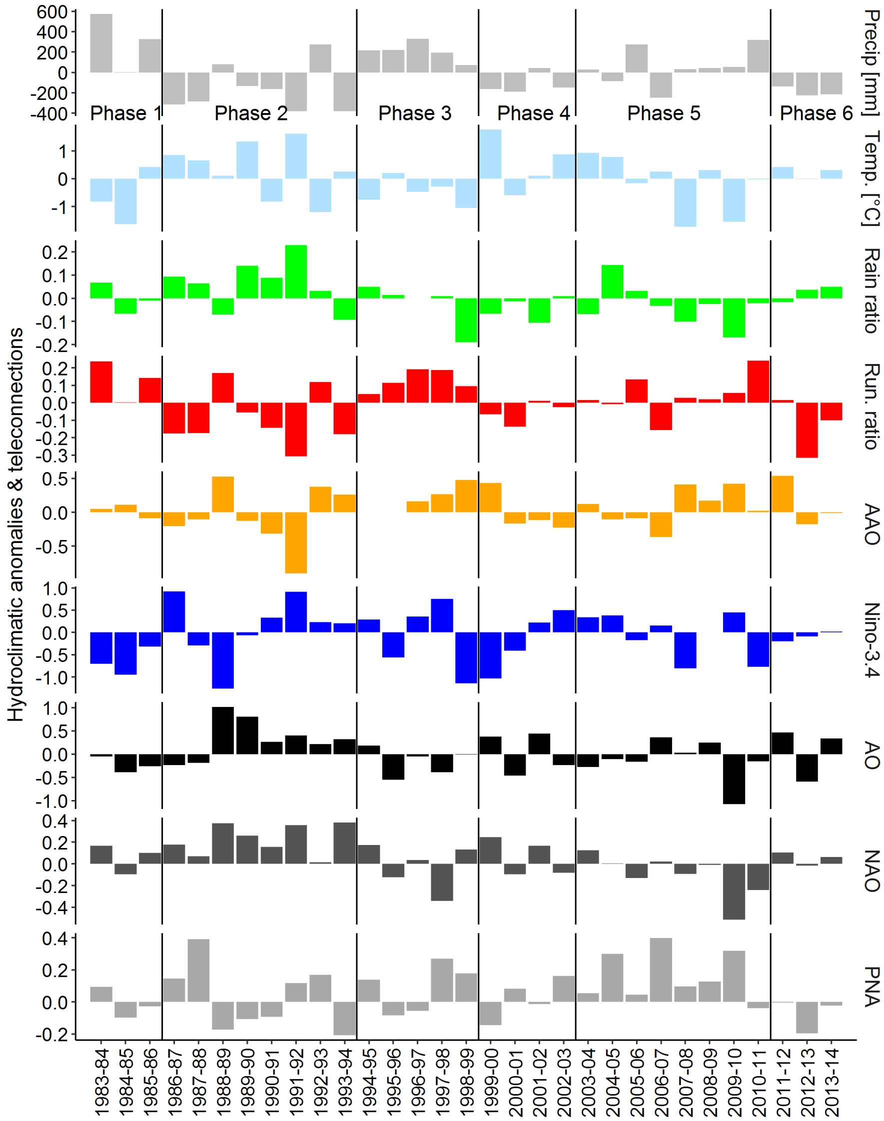
Phase 1
Phase 2
Phase 3
Phase 4
Phase 5
Phase 6
Precip [mm]
Temp. [°C]
Rain ratio
Run. ratio
AAO
Nino-3.4
AO
NAO
PNA
Hydroclimatic anomalies & teleconnections
1983-84
1984-85
1985-86
1986-87
1987-88
1988-89
1989-90
1990-91
1991-92
1992-93
1993-94
1994-95
1995-96
1996-97
1997-98
1998-99
1999-00
2000-01
2001-02
2002-03
2003-04
2004-05
2005-06
2006-07
2007-08
2008-09
2009-10
2010-11
2011-12
2012-13
2013-14

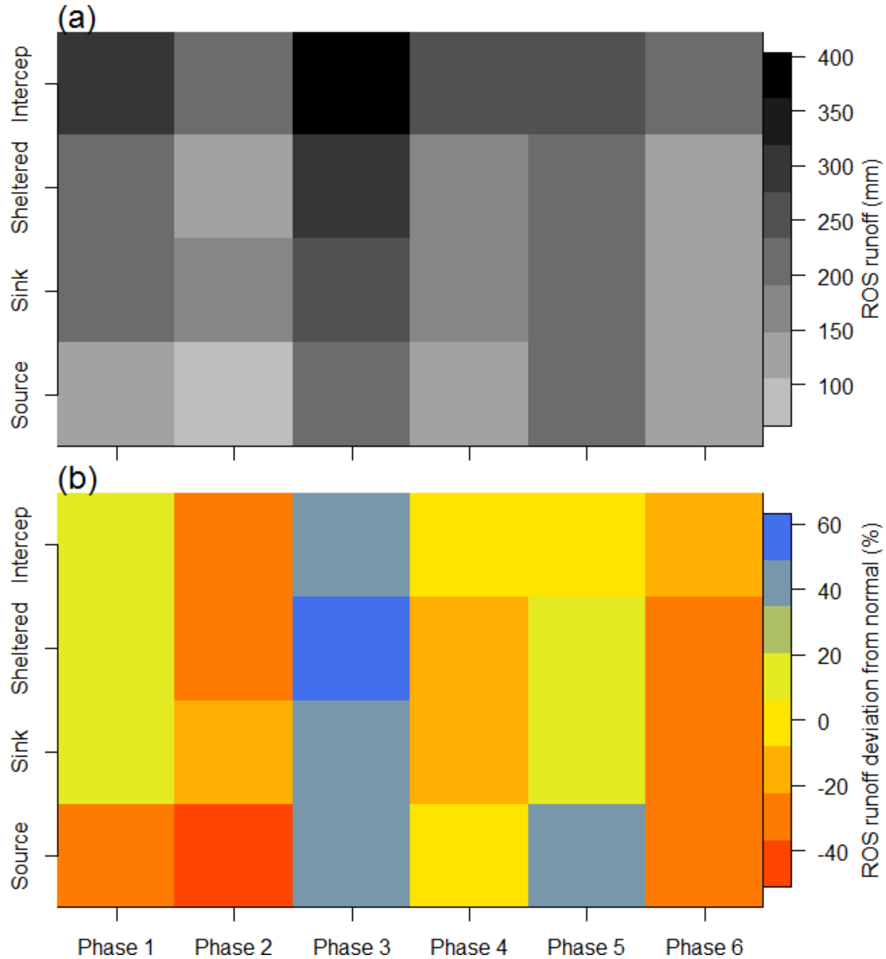
(a)
Intercep
Sheltered
Sink
Source
400
350
300
250
200
150
100
ROS runoff (mm)
(b)
Intercep
Sheltered
Sink
Source
60
40
20
0
-20
-40
ROS runoff deviation from normal (%)
Phase 1
Phase 2
Phase 3
Phase 4
Phase 5
Phase 6

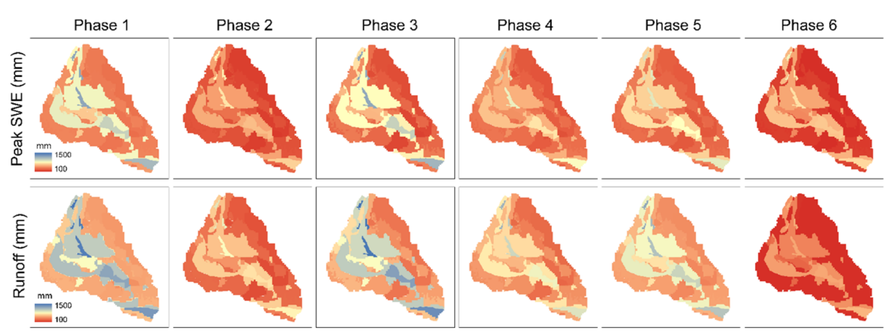
Phase 1
Phase 2
Phase 3
Phase 4
Phase 5
Phase 6
Peak SWE (mm)
Runoff (mm)